Sensors & Diagnostics

TUTORIAL REVIEW

View Article Online
View Journal | View Issue

Cite this: *Sens. Diagn.*, 2025, **4**, 293

Reactivity-based small-molecule fluorescence probes for sensing biogenic amine cadaverine – a biomarker to determine food freshness

Mannanthara Kunhumon Noushija, Alenthwar Vamshi Krishna, Ruhila Taj Mehboob Ali and Sankarasekaran Shanmugaraju *

The design and fabrication of sensor probes to check food freshness and assess food quality is an essential area of research. Every year, millions of people are affected by food poisoning and fall victim to foodborne-related health problems. Cadaverine (1,5-pentanediamine) is a biogenic amine and an important biomarker to determine food freshness. Measuring cadaverine concentration allows us to assess the quality and freshness of food. Recently, fluorescence-based sensing methods have been used extensively as a viable probe to measure cadaverine concentrations. In this review article, we have summarized reactivity-based small-molecule fluorescence chemosensors reported to date for sensing and quantification of cadaverine. We provide a detailed discussion of the design, synthesis, and fluorescence-sensing properties of several small-molecule sensors employed for cadaverine detection. Lastly, the limitations of existing fluorescence sensors and our view on future perspectives for developing practically useful fluorescence sensor systems for real-time monitoring of the concentrations of cadaverine biomarkers have been stated. Given its importance, this review article will attract and greatly benefit scientists working in related research areas.

Received 29th November 2024,
Accepted 26th February 2025

DOI: 10.1039/d4sd00358f

rsc.li/sensors

1. Introduction

Food safety and public health are strongly intertwined, which constantly raises concerns all over the world. As stated by the World Health Organization (WHO), consuming unhygienic food causes the spread of more than 200 diseases from cancer to diarrhoea.[1] Each year, millions of individuals are affected by food poisoning and contract various foodborne illness.[2] The actual numbers are greater since it can be challenging to prove a link between food contamination and sickness or death, which means that many occurrences of foodborne disease go unreported or unrecorded.[3] This emphasizes the need to ensure that our food is free of contaminants that might be hazardous and toxic to human health. The most common food contaminants are viruses,

Department of Chemistry, Indian Institute of Technology Palakkad, Palakkad-678623, Kerala, India. E-mail: shanmugam@iitpkd.ac.in

Mannanthara Kunhumon Noushija

Ms. Mannanthara Kunhumon Noushija is a Ph.D. student at the Indian Institute of Technology Palakkad. She completed her M.Sc. in Chemistry from Calicut University campus, Thenhippalam, and her B.Sc. in Chemistry from Government Victoria College Palakkad. Her research interests are the design of small-molecule-based fluorescence chemosensors for biologically related analytes.

Alenthwar Vamshi Krishna

Mr. Alenthwar Vamshi Krishna received a BS-MS dual degree in Chemistry from the Indian Institute of Science Education and Research (IISER), Pune, in 2019. He is now pursuing a Ph. D. in Chemistry at the Indian Institute of Technology Palakkad. His research is focused on developing polyimide-based cathode materials for battery applications.

fungi, bacteria, parasites, toxic heavy metals, and pesticides.[4] Rather than harmful chemicals, food poisoning is mostly caused by germs and pathogens.[5] But all of this might occur due to unhygienic surroundings and insufficient care. Therefore, checking the freshness of food is significant and essential to avoid foodborne related health issues. Biogenic amines (BAs) mainly arise as food spoilage indicators. They are generally produced from decarboxylase's microbial decomposition of free amino acids, resulting in serious toxicological risks and food poisoning.[6] Especially in the case of foods such as meat, seafood, fish, wine, and cheese, the natural degradation of proteins causes the release of BAs including ammonia, putrescine, cadaverine, dimethylamine, trimethylamine, histamine, and methyl amine.[7,8] Amination and transamination of aldehydes and ketones can produce several additional amines. Moreover, nitrosamine, a substance that causes cancer, is created when BAs react with the nitrites found in meat.[9]

Across the world, both buyers and sellers are having serious problems with the freshness of meat and its deterioration. Eating spoiled meat can cause several disorders, such as cancer, nausea, vomiting, and stomach pain. In extreme circumstances, it may cause heart failure and even death.[10,11] Thus, customers place a high priority on the freshness of meat products. The biogenic diamine (BA) such as cadaverine (1,5-pentanediamine) produced through microbial enzymatic decarboxylation of amino acids, has frequently been used as a target analyte to monitor meat freshness. They are significant in the food industry and the biomedical field because they are the most visible indicators and the source of the foul odour caused by meat decomposition. Further, cadaverine has been linked to a variety of human diseases such as lupus erythematosus,[12] uterine cancer,[13] and liver damage.[14] So, in the current situation, the detection and quantification of cadaverine finds enormous relevance.

To detect cadaverine, several analytical techniques have been developed, including high-performance liquid chromatography,[15,16] gas chromatography coupled with mass spectra,[17] electrochemical methods,[18] quartz crystal microbalance, ion mobility spectrometry, the colorimetric method,[19,20] and chemiresistive sensors. Unfortunately, these techniques cannot check on-site meat freshness since they usually need more time and expensive equipment.[21,22] Moreover, their sample preparation is much more complex. An accurate, practical, and affordable technique to evaluate meat quality is essential. Because of its advantages over other sensing approaches, such as high selectivity and sensitivity, rapid response, real-time and visual monitoring of an analyte, less expense, quick response, lower background interference, and simple operation, fluorescent sensing has become an increasingly appealing analytical method.[23–28] Among fluorescent sensors, small molecule fluorescent probes are interesting because of their structural diversity, high-yield synthesis, good reproducibility in synthesis, and excellent sensing performances. Further, the sensing propensity of small-molecule fluorescence sensors can even be modulated by introducing suitable substituents. Within small-molecule probes, more focus has been given to fluorescent probes that use a chemical interaction between the analyte and the sensing probe. Upon the analyte addition, the structural changes to the sensor chromophore during a chemical reaction might result in significant photophysical changes visible to the human eye.

There are a few comprehensive reviews of the fluorescent sensors for BAs detection where BA serves as a nucleophilic

Ruhila Taj Mehboob Ali

Ms. Ruhila Taj Mehboob Ali obtained her B.Sc. and M.Sc. degrees in Chemistry from PSGR Krishnammal College for Women, Coimbatore. Currently, she is a Ph.D. student working in the Department of Chemistry at the Indian Institute of Technology Palakkad. Her research interests include the design and synthesis of luminescent organic structures and organometallic complexes for applications in biomedicine.

Sankarasekaran Shanmugaraju

Dr. Sankarasekaran Shanmugaraju received his B.Sc. and M.Sc. degrees in Chemistry from The American College, Madurai, and his Ph.D. degree with a gold medal for the best thesis in Inorganic Chemistry from the Indian Institute of Science (IISc), Bengaluru. In 2014, he moved to Trinity College Dublin, Ireland, as an Irish Research Council (IRC) postdoctoral fellow. In October 2018, he joined the Department of Chemistry as an Assistant Professor at the Indian Institute of Technology Palakkad. Since June 2023, he has been an Associate Professor in the same institution. His group's current research activities are supramolecular structures & functional materials and sensor chemistry.

reagent and base.[29–31] However, there is no detected review article on reactivity-based small molecule fluorescent probes for cadaverine detection. Cadaverine could undergo various chemical reactions including Schiff base formation, ester aminolysis, amine exchange, and nucleophilic addition. In the past, several fluorescent probes with different functional groups including aldehyde,[32,33] anhydrides,[34,35] and ester,[36–38] have been developed to detect cadaverine. This article aims to discuss various small-molecule-based cadaverine sensors reported to date. We provide a detailed discussion of the design, synthesis, and reactivity-based fluorescence-sensing properties of several small-molecule probes employed for cadaverine sensing. We have also included sensors that could detect other BAs along with cadaverine. We believe this review will give a future perspective on further development of sensors for specifically sensing cadaverine.

2. Reactivity-based small-molecule fluorescence probes for sensing cadaverine

In the year 2003, Feuster and Glass investigated a family of fluorescent coumarin-containing sensors with formyl (–CHO) groups to specifically sense amine-containing analytes (amines and amino acids) because amines can spontaneously form an iminium ion, which consequently changes the fluorescent characteristics of the coumarin core.[38] Inspired by this study, in 2005, the same group reported a set of seven small-molecule fluorescent sensors **1a–g** based on dimers of a quinolone aldehyde chromophore for diamine guests detection (see Fig. 1A for structures).[33] The aldehyde-containing sensors are known to react with diamine to form a 1 : 1 bis-iminium ion adduct (Fig. 1B). Butylamine, diamino propane, diamino butane, diamino pentane (cadaverine), ornithine, and lysine are the amines that were used as analytes. A good binding constant and outstanding fluorescence enhancements were observed for these sensors towards different amine guests in a partially aqueous methanol solution. Additionally, useful selectivity of sensors for various lengths of amines was achieved by altering the linker unit of sensor molecules. When diamine guests were mixed with the sensor's solution, a significant red-shift in the absorption maximum was observed, due to the intermolecular hydrogen bonding between the iminium ion produced and the chromophore's carbonyl group. Interestingly, upon excitation at λ = 495 nm, the fluorescence emission intensity of sensors was drastically increased after titrating with the diamine guests. All of the dialdehyde sensors were predicted to bind to most diamines at the outset, still shorter linkers were found to prefer short-chain diamines over long-chain diamines and *vice versa*. Moreover, amines that do not suit the binding length of the sensor were found to exhibit poor fluorescence sensing responses. All the sensors **1a–1g** showed a good fluorescence sensing response for cadaverine and the binding constant was determined to be in the range of K_a = 270 to 2200 M^{-1}. Among these, sensor **1g** with pentane linker had a greater binding constant and thus, high selectivity for cadaverine over other diamine guests.

Motivated by the work of Glass, Severin *et al.* developed a coumarin-based small-molecule sensor **2** for cadaverine sensing in a buffered aqueous solution (50 mM HEPES, pH 7.4) (see Fig. 2, inset).[39] Sensor **2** displayed an absorption band at λ = 451 nm, which was diminished in the presence of an amine (histidine, cysteine, histamine, cadaverine, and

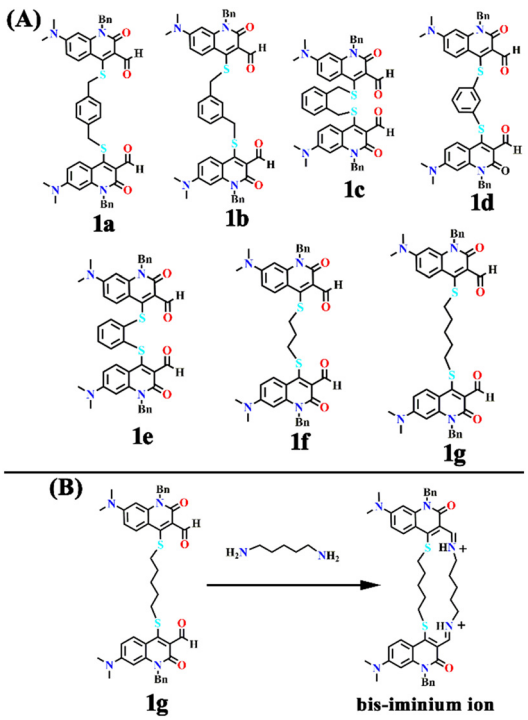

Fig. 1 (A) The structure of quinolone aldehyde-based sensors **1a–g** and (B) the proposed reactivity-based sensing of cadaverine by sensor **1g**.

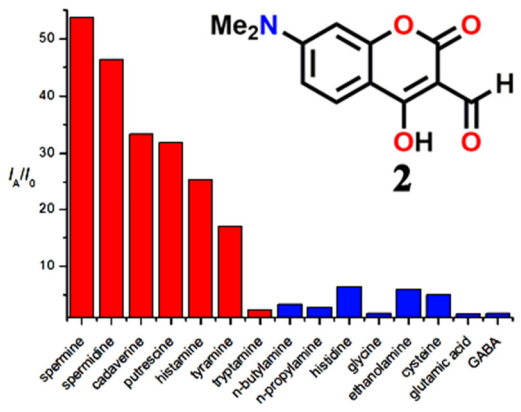

Fig. 2 The changes in fluorescence emission intensity at λ = 472 nm of sensor **2** in the presence of different amines (inset: the structure of sensor **2**). Reproduced with permission from ref. 39. Copyright 2011, Royal Society of Chemistry.

spermine), and a new set of peaks at λ = 377 and 400 nm emerged. The variations in the absorption spectra of **2** were distinct for each of the five amines, with spermine and cadaverine showing the most pronounced changes. To corroborate the selectivity of **2** for BA, UV-visible absorption studies were carried out using several amine guests, and variations in the absorption spectra of **2** at λ = 403 and 377 nm were monitored. It was concluded that λ = 403 nm serves as a selective indication of the existence of BA. Even though the selectivity for BAs over other amines at λ = 377 nm was not as high as that seen at λ = 403 nm, it was still impressive. Similar results were seen in the fluorescence titration studies. Upon excitation at λ = 377 nm, sensor **2** exhibited fluorescence emission at λ = 470 nm; the intensity of this peak was significantly increased for samples containing BAs (0.5 mM) (Fig. 2). However, the apparent selectivity of **2** for cadaverine and other BAs over amino acids and other simple primary amines was unclear. It was further demonstrated that sensor **2** can detect BAs in micromolar (μM) concentrations and gaseous amines when integrated into a polymer matrix.

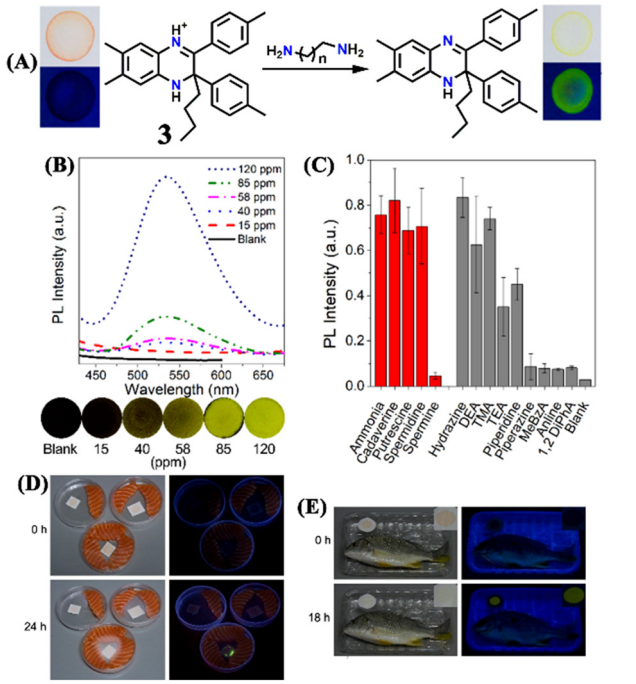

Fig. 3 (A) The conversion of the protonated form of sensor **3** to its deprotonated form after exposure to BAs (inset: the original red colour of **3** changed to bright yellow after exposure to BAs). (B) The photoluminescence spectra of **3** loaded filter paper strips exposed to different concentrations of ammonia vapours and the corresponding photographs were imaged under UV light irradiation. (C) The turn-on photoluminescence responses of **3** loaded filter paper strips after exposure to different amine vapours (red bar = BAs, grey bar = other amines). (D) The observed fluorescence emission enhancement for **3** (after 24 h exposure) sealed with salmon sashimi. (E) Turn-on fluorescence responses were observed for **3** after 18 h exposure in a sealed package of yellowfin seabream. Reproduced with permission from ref. 40. Copyright 2017, Willey.

1,2-Dihydroquinoxaline derivatives are an interesting class of fluorophores that exhibit noticeable changes in photoluminescence properties when an interconversion between protonated and deprotonated forms occurs. Based on this, in the year 2017, Tang *et al.* designed and used a protonated form of a 1,2-dihydroquinoxaline sensor **3** for the sensitive detection of cadaverine and other BAs like putrescine and spermidine (Fig. 3A).[40] The deprotonated form **3** displayed solvent polarity-dependent fluorescence emission and aggregation-induced emission (AIE) characteristics. Sensor **3** was red, absorbed at λ = 338 and 478 nm, and had emission maxima at λ = 560 nm in DCM. Photoinduced electron transfer (PET) and the self-absorption phenomena made probe **3** non-emissive, which becomes emissive upon deprotonation when exposed to cadaverine or other BAs (Fig. 3A). **3** loaded filter paper strips were made and used for cadaverine detection. The original red colour of **3** changed to yellow along with a strong fluorescence emission under UV light when paper strips were exposed to BAs (Fig. 3B). The bright yellow fluorescence was observed within 40 seconds of amine exposure. The increased fluorescence emission was ascribed to the AIE property of **3**. Similar changes and good sensitivity were seen for other amines including putrescine, spermidine, hydrazine, triethylamine (TEA), diethylamine (DEA), trimethylamine (TMA), and piperidine (Fig. 3C). Moreover, probe **3** was shown to detect ammonia vapour with an appreciable detection limit of 690 ppb. The paper-strips-based sensing was further extended to *in situ* detection of BAs generated from food fermentation (Fig. 3D and E). Sensor **3** loaded test strip was sealed with fresh salmon sashimi and yellowfin seabream packages. The colour and emission of test strips were visually changed after one- or two-day exposure. The original red colour of the strip changed to bright yellow and fluorescence emission was enhanced. These apparent colour changes and fluorescence turn-on confirmed that the

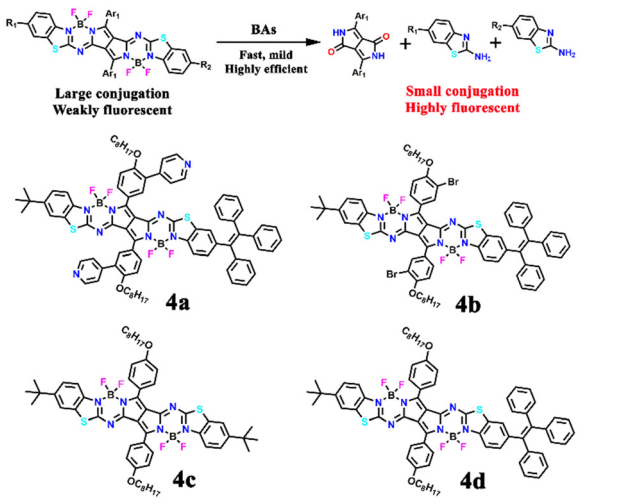

Fig. 4 The proposed detection mechanism for the sensing BAs using pyrrolopyrrole aza-BODIPY and the structure of sensors **4a**–**4d**.

appreciable level of BAs had been produced by fermentation. All these observations demonstrated the practical use of sensor **3** for *in situ* detection and monitoring of the concentration of BAs and thus determine the food spoilage.

In another report, Ran *et al.* designed four pyrrolopyrrole aza-BODIPY (PPAB) sensors **4a–4d** for ultrasensitive and highly selective detection of BAs (Fig. 4).[41] The large conjugated structure of the PPAB sensor contains B–N bonds, due to the high nucleophilicity, which undergoes bond cleavage in the presence of amine guest and subsequent transimination and hydrolysis results in the generation of smaller conjugated molecules (Fig. 4). The conversion of larger conjugated PPAB derivatives to small conjugated systems causes a λ = 225 nm hypsochromic shift in the absorption maximum and 12-fold fluorescence enhancement.

In dioxane solvent, **4a–4d** exhibited a shoulder band with an absorption maximum at λ = ~630/675 nm and two weak emission peaks at about λ = 700 and 525 nm. The mechanism of amine detection was explored using **4a** as a representative probe. Among different amine guests, **4a** displayed selective fluorescence "turn-on" responses to BAs, particularly for cadaverine, ethylenediamine, and putrescine (1,4-butanediamine) within a short reaction time. A noticeable colour shift from green to yellow and significant changes in the fluorescence emission was observed within one minute of mixing an equimolar combination of diamines and **4a** in dioxane at room temperature. The low-energy peak λ = 700 nm disappeared and the high-energy peak at λ = 550 nm became stronger with longer reaction times (Fig. 5). The conversion of one emissive species to another was supported by a clear isosemissive point with a well-defined center at around λ = 650 nm. Upon mixing BAs with **4a**, the two absorption bands at λ = 630 and 675 nm vanished and a new blue-shifted peak in the range from 425 to 450 nm emerged (Fig. 5). Two clear isosbestic points at λ = 505 and 431 nm revealed the formation of new species. The reaction between BAs and **4a** followed the pseudo-first-order kinetics and the rate constant for cadaverine was K_a = 3.15 × 10^{-3} s^{-1}. The high selectivity of **4a** for BAs was further established by titration with other competing analytes. The mixing of other amines and reagents like amide, dicarboxylic acid, ester, diol, and alkyl halides showed no reaction with **4a**. The limit of detection (LoD) for 1,3-propanediamine, putrescine, and cadaverine was found to be 2.46 ppb, 3.14 ppb, and 3.28 ppb, respectively. These values are significantly lower than other reported small-molecule fluorescent sensors. Additionally, the fish freshness was checked using **4a**-loaded test strips and film forms (Fig. 5), demonstrating the practical utility of the sensors. These findings highlight the potential use of low-cost, quick-responding PPAB sensors for detecting fish spoilage. In continuation, by the same group, a novel PPAB-based probe for effective colorimetric and fluorescent sensing of BAs was reported.[42] The reaction between lactam-fused aza-BODIPY dye and polyamines (spermidine, spermine, and cadaverine) produced a noticeable colour change from pink to yellow and significant fluorescence quenching in less than a minute.

Based on a highly efficient condensation–cyclization cascade reaction, in 2020, Zhu *et al.* developed a novel colorimetric and fluorescence lighting-up probe **5**.[43] Probe **5** consists of vicinal chloro and formyl groups in the diethylamino coumarin skeleton, which undergoes a reaction with cadaverine to form a cyclic structure (see Fig. 6A). The rigid planar structure of the product resulted in strong colorimetric and fluorescence lighting-up responses. Upon increasing the concentration of cadaverine, the strong absorption band of **5** at λ = 450 nm decreased, which was accompanied by the appearance of a new band at λ = 375 nm with a clear isosbestic point centered at λ = 400 nm and an observable colour change from yellow to colourless (Fig. 6B).

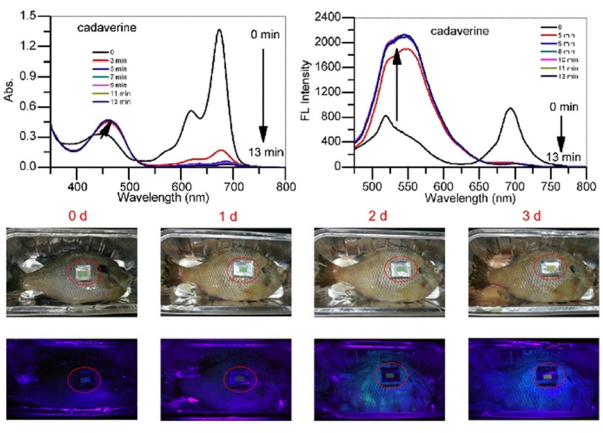

Fig. 5 The time-dependent UV-visible absorption (top left) and fluorescence emission (top right) spectra for sensor **4a** in the presence of cadaverine (40 equiv.) in dioxane. The fish spoilage monitoring using **4a**-loaded filter paper. Reproduced with permission from ref. 41. Copyright 2020, Elsevier.

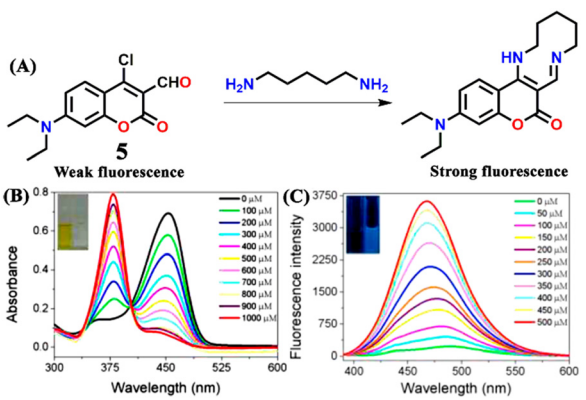

Fig. 6 (A) The structure of sensor **5** and its reaction with cadaverine produces a rigid cyclic product exhibiting strong fluorescence emission. (B) The change in the UV-visible absorption spectra of **5** after increased mixing of cadaverine (inset: colour changes seen under room light). (C) The increased fluorescence emission for **5** upon increased addition of cadaverine (inset: colour changes seen under UV light). Reproduced with permission from ref. 43. Copyright 2021, Elsevier.

The heavy atom effect was attributable to the non-fluorescent nature of the probe, which gets altered by reaction with cadaverine since it forms a cyclic structure with strong blue fluorescence emission. The emission band of **5** at λ = 475 nm gradually increased in intensity with increasing concentrations of cadaverine (Fig. 6C). A similar result was obtained for putrescine over other interfering species like nucleophilic amines, anions, and biothiol species. Probe **5** showed a rapid sensing response, excellent selectivity, and good sensitivity to the typical biogenic aliphatic primary amines; cadaverine, and putrescine, with a low LoD of 209 nM. Also, **5** loaded test papers were developed for the real-time monitoring of biogenic primary diamines during fish spoiling.

Kim and co-workers synthesized amine-reactive activated esters of *meso*-carboxy BODIPY sensors **6a** and **6b** which react with aliphatic amines to form amides (Fig. 7A).[44] Weakly fluorescent ester compounds **6a** and **6b** became highly fluorescent through ester-to-amide conversion. Both probes exhibited the same emission maxima at λ = 615 nm in acetonitrile, but **6a** showed an absorption band at λ = 541 nm, while **6b** showed a peak at λ = 534 nm. **6a** exhibited drastic spectral changes upon the addition of methylamine. When methylamine was added, the original absorption and emission spectra were reduced, and new blue-shifted bands emerged. Moreover, the sensor showed the most significant fluorescence response (F/F_0 > 2250 within 5 minutes) and high kinetic sensitivity to cadaverine and other primary amines (methylamine, 1-butanamine, 1-hexanamine, 1,3-diaminopropane, and putrescine). The bulk primary amines showed less intense sensing responses and the highly hindered amines showed no notable emission responses. Further, the solid-state sensing properties were explored by depositing the **6a** probe into filter strips and using it for monitoring the fish's freshness (Fig. 7B). The luminescence of the probe progressively turned from red to yellow over 12 hours of incubation at room temperature, together with a colour change from pink to orange, demonstrating its potential utility in food quality and safety monitoring. For

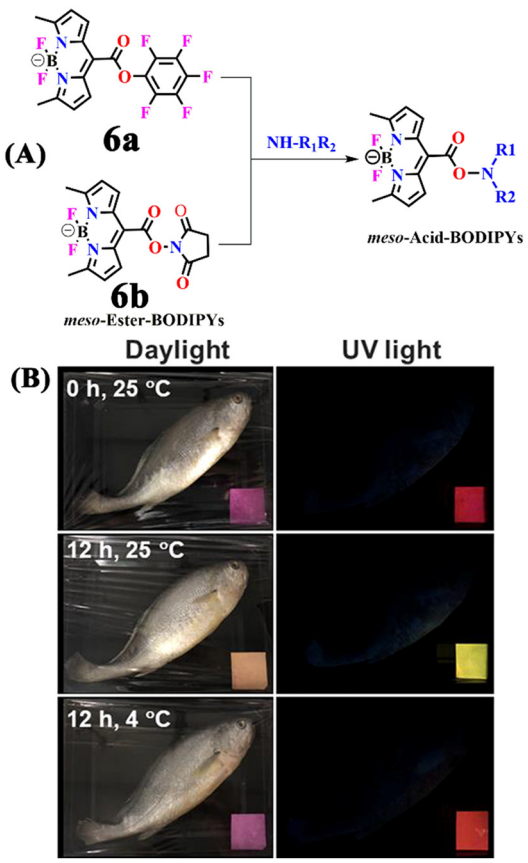

Fig. 7 (A) Sensors **6a** and **6b** and the proposed BA sensing mechanism through ester-to-amide conversion. (B) Monitoring white croaker fish freshness using **6a** leaded filter paper imaged (in daylight and under UV light) at different time intervals and incubation temperatures. Reproduced with permission from ref. 44. Copyright 2020, American Chemical Society.

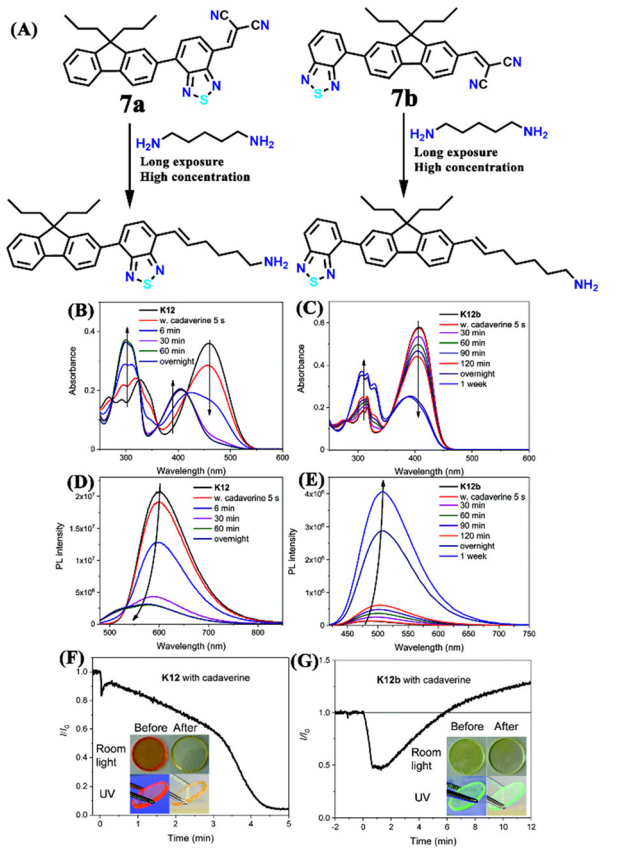

Fig. 8 (A) Sensors **7a** and **7b** and their aza-Michael addition reaction with cadaverine at high concentration. The change in electronic absorption spectra of (B) **7a** (labeled as K12) and (C) **7b** (labeled as K12b) were recorded at different exposure intervals after cadaverine addition. The change in fluorescence emission spectra of (D) **7a** (labeled as K12) and (E) **7b** (labeled as K12b) were recorded at different exposure intervals after cadaverine addition. The change in photoluminescence peak intensity of (F) **7a** (labeled as K12) and (G) **7b** (labeled as K12) loaded thin films after exposure to cadaverine vapours at different exposure times (inset: corresponding photographs imaged in daylight and under UV light). Reproduced with permission from ref. 45. Copyright 2020, Royal Society of Chemistry.

primary amines, it was possible to obtain considerable alterations in emission maxima and an increase in fluorescence intensity of up to 3000%. The selective fluorogenic detection and labelling of primary amines, amino acids, and proteins, the detection of food spoilage, and the staining of proteins on electrophoretic gels or in live cells were further proven based on this quick and efficient procedure.

Zhang *et al.* reported two isomeric fluorine benzothiadiazole-based fluorescent probes, **7a** and **7b**, which comprise dicyanovinyl moieties as their active sites for BA sensing (Fig. 8A).[45] The sensors differ in the position of dicyanovinyl groups, which undergo an aza-Michael addition with the amine group of cadaverine (Fig. 8A). Time-dependent colorimetric and fluorescence responses of sensors were recorded in the solution and solid state by fabricating thin films through the spin-coating process. The high electrophilic nature of the vinyl group in **7a** made the sensor more reactive towards amine than **7b**. UV-visible absorption spectral observations revealed that both sensors have two absorption maxima, and the intensity of the higher wavelength band decreases and the lower wavelength band increases with the addition of cadaverine, along with a blue shift in the long-wavelength absorption band (Fig. 8B and C). The blue shift in both cases indicated the formation of a new species with lesser conjugation. When it comes to the fluorescence spectra, turn-off and turn-on responses were observed for **7a** and **7b**, respectively, upon adding cadaverine to the solution state (Fig. 8D and E). On the other hand, in the solid state, when the cadaverine vapour initially diffuses into the film, the photoluminescent intensity of **7a** attenuated by 50% in 200 s due to photoinduced hole transfer, which happens on a considerably quicker timescale than aza-Michael addition (Fig. 8F). The subsequent aza-Michael addition caused 90% fluorescence quenching over time. Using a similar two-step sensing system, the **7b** thin film also showed an initial decrease in fluorescence intensity (50% decreased after 38 s exposure), followed by a slow rise to considerably beyond the original value (Fig. 8G). Significant photo-induced hole transfer quenching of diethylamine and triethylamine was discovered without any chemical transformation process. For solid-state films based on **7a** and **7b**, the LoD for cadaverine was 130 ppb and 610 ppb, respectively. The practical applicability of the sensors was further demonstrated by showing the response of the films toward the vapours released during prawn spoilage.

Monteiro-Silva and his group prepared catechol-derived Rosamine dyes through a microwave-assisted method for BA sensing (Fig. 9A).[46] Among the two novel 2,3- and 3,4-dihydroxy phenyl substituted rosamines, the latter probe **8** showed significant sensing properties toward cadaverine, butylamine, and putrescine. When two equivalents of amine were added to the sensor **8** solution in acetonitrile, the absorption intensity of the band at λ = 552 nm decreased; this change was more prominent for cadaverine (Fig. 9B). Similarly, two equivalents of amine quests elicited a significant quenching of emission intensity at λ = 573 nm, except for *t*-butylamine, which showed a little enhancement in the emission intensity (Fig. 9C). With cadaverine, the percentages of enhanced fluorescence and decreased absorbance were 18% and 29%, respectively. In addition, the gas-phase sensing study was done to verify that sensor **8** can be applied for fish freshness assessment. Interestingly, the gas-phase sensing displayed a higher percentage of quenching than in the solution state. Almost, 47% of fluorescence quenching was observed for cadaverine. The possible mechanism of sensing of **8** was ascribed to the nucleophilic attack of the amine quest on the electrophilic 9-position of the xanthene yielding an addition adduct and subsequent loss of catechol moiety.

In 2022, Kim and co-workers reported a series of fluorescent probes (**9a–c**) based on julolidine-fused coumarin adorned with different electron-withdrawing substituents (Fig. 10A).[47] They used the sensors to test the freshness of the meat by selectively sensing the cadaverine. The sensing mechanism revealed that probes undergo aza-Michael addition following an elimination reaction with cadaverine to produce a colorimetric and a ratio metric fluorescence response (Fig. 10B). The electron-withdrawing substituents were introduced on the core moiety to improve the sensing capability. Among the three sensors, **9a** with a dicyanovinyl unit exhibited a rapid sensing response (~60 s) and an enhanced sensing performance. The low LoD of 14 nM indicated the high sensitivity of **9a** towards cadaverine. The sensing properties were probed using UV-visible absorption and fluorescence titration studies. The absorption band of **9a** appeared at λ = 560 nm, and its intensity decreased with the addition of cadaverine (Fig. 10C). Meanwhile, they observed the simultaneous generation of a new band at λ = 541 nm. Similarly, the fluorescence emission peak of **9a** at λ = 604 nm disappeared with the appearance of a new band at λ = 504

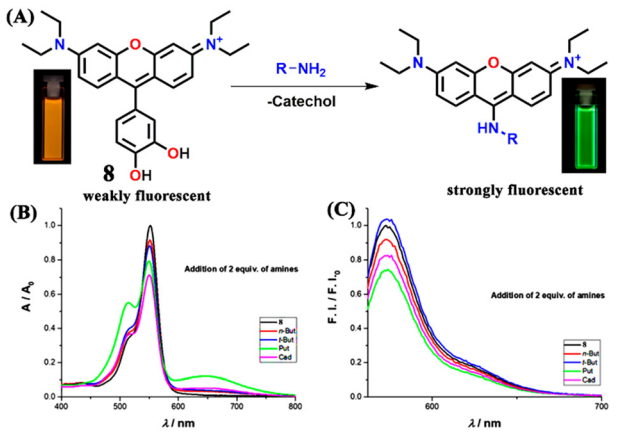

Fig. 9 (A) Sensors **8** and its reaction with the BA to fluorescent addition adduct after the loss of catechol moiety (inset: the orange colour of **8** changed to bright green after reaction with an amine). The changes in UV-visible absorption (B) and fluorescence emission (C) spectra of **8** in the presence of two equivalents of different amines. Reproduced with permission from ref. 46. Copyright 2021, MDBI.

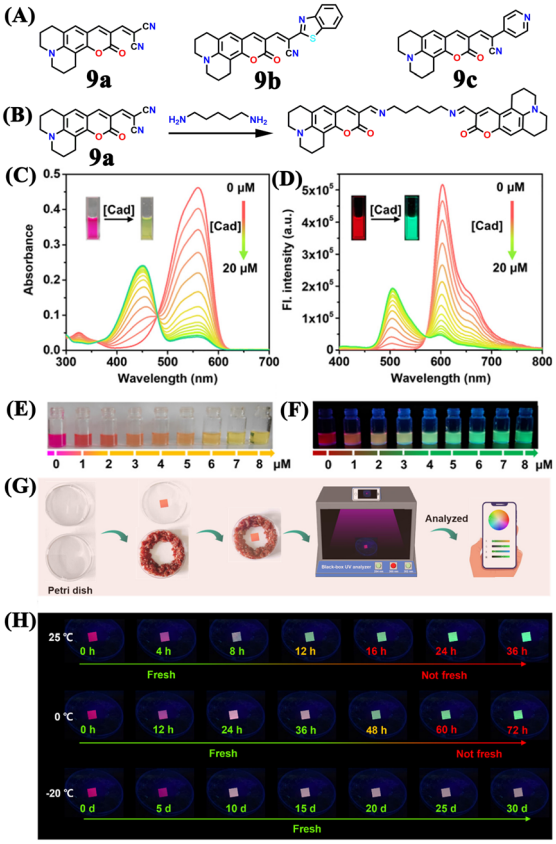

Fig. 10 (A) The structure of sensors **9a–c** and (B) mechanism of cadaverine sensing by sensor **9a**. The changes in (C) UV-visible absorption and (D) fluorescence emission for **9a** upon the gradual mixing of cadaverine (inset: corresponding colour changes). The visual colour changes were seen for sensor **9a** in the presence of cadaverine at different concentrations, imaged (E) in room light and (F) under UV-light irradiation. (G) The schematic representation of the procedure used for monitoring the beef freshness. (H) The fluorescence images of **9a**-loaded test strips sealed with beef were imaged at different temperatures at different times and under UV-light irradiation. Reproduced with permission from ref. 47. Copyright 2022, American Chemical Society.

nm with a clear isosbestic point at λ = 570 nm upon the gradual addition of cadaverine (Fig. 10D). Moreover, **9a** was fabricated into test kits to detect cadaverine vapour since it showed visual colour change and fluorescence transition from red to green (Fig. 10E and F). On-site monitoring of meat freshness without contacting and destroying the sample was effectively accomplished using two-colour imaging of cadaverine vapour (Fig. 10G and H). Because of their effective sensing capabilities, **9a** test kits can be a viable real-time fluorescence screening platform for a quick, non-destructive, and precise assessment of meat freshness.

Another dicyanovinyl-based sensor **10** was introduced by Min *et al.* for specifically detecting cadaverine (Fig. 11A).[48] They proposed that sensing of cadaverine was based on the reversed Knoevenagel condensation mechanism. The absorption and emission studies were carried out in a DMSO medium to demonstrate the cadaverine sensing performance

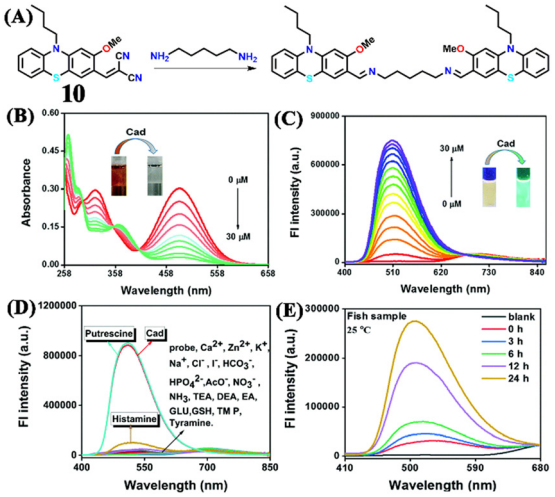

Fig. 11 (A) The structure of sensor **10** and its reaction with cadaverine. The observed changes in (B) absorption and (C) fluorescence emission spectra of **10** upon the addition of cadaverine in increased concentrations (inset: corresponding visual colour changes). (D) The fluorescence spectra of **10** in the presence of cadaverine and other competing analytes. (E) The fluorescence spectra of **10** after mixing cadaverine extracts from fish samples exposed at 25 °C at different times. Reproduced with permission from ref. 48. Copyright 2022, Royal Society of Chemistry.

of **10.** The intensity of the strong absorption band at λ = 472 nm gradually decreased with the incremental addition of cadaverine, accompanied by a visible colour change from brown to colourless (Fig. 11B). The emission spectra consisted of a weak band at λ = 704 nm, which gets diminished upon the addition of cadaverine, with simultaneous generation of a new band at λ = 512 nm with higher intensity (Fig. 11C). Common cations, anions, and biomolecular species did not cause any spectrum alterations, which confirmed the high selectivity of **10** for cadaverine (Fig. 11D). But putrescine caused a considerable fluorescence amplification (Fig. 11D). These results indicated that **10** could be employed as a colorimetric probe that quantitatively determines cadaverine and putrescine. They demonstrated the practical utility of **10** by fabricating smart tags and using them for cadaverine vapour detection to determine fish freshness. They performed on-site monitoring of the fish freshness without sample destruction by keeping the fish for different storage times (0–24 h) under 0 °C and 25 °C (Fig. 11E). Excellent sensing performance towards cadaverine vapours within a short time was achieved. Moreover, the smartphone-adaptable chromaticity diagram was developed for on-site digital fish freshness monitoring. The LoD was found to be 46 nM, and that of cheap and portable sensing tags was determined to be 8.65 ppm, which exhibited a colour change from red to green in the presence of cadaverine vapours.

Another interesting biocompatible and highly fluorescent resorufin dye-based "turn-on" sensor **11** was developed for cadaverine and putrescine detection (Fig. 12A).[49] The detection was primarily attributed to the

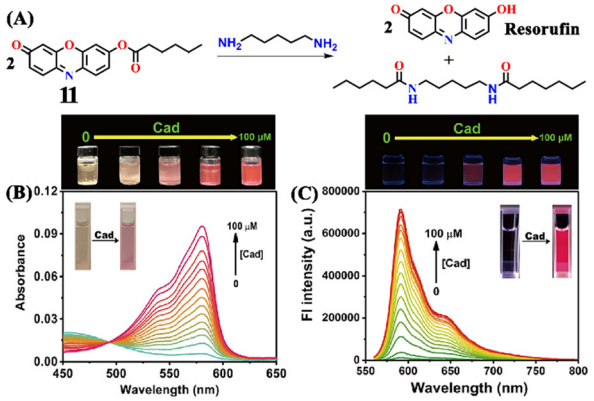

Fig. 12 (A) The structure of sensor **11** and its reaction with cadaverine yield red-emissive resorufin dye. The changes in (B) absorption and (C) fluorescence emission spectra of **11** upon the addition of cadaverine in increased concentrations (inset: corresponding visual colour changes). The above images correspond to colour changes for different concentrations of cadaverine. Reproduced with permission from ref. 49. Copyright 2023, Elsevier.

liberation of resorufin dye after removing the caproyl group from **11** by cadaverine or putrescine (aminolysis), which was distinctly evident by a colour transition from colourless to pink (Fig. 12A–C). The colourless sensor **11** initially exhibited a weak absorption band between λ = 450 and 620 nm; however, with the introduction of cadaverine, a distinct absorption peak emerged at λ = 578 nm (Fig. 12B). Due to the presence of the caproyl ester, **11** was initially non-fluorescent ($\Phi_f < 0.002$) in the DMSO/PBS buffer. However, the non-fluorescent sensor turned red-emissive with a new peak at λ = 592 nm (Fig. 12C). **11** showed high selectivity and sensitivity for cadaverine with a LoD of 89.2 nM. Further, **11** was integrated into test strips and a smart tag, allowing non-contact, non-destructive assessment of seafood freshness. Following exposure to cadaverine vapour, the test strips showed a distinct colour change from colourless to pink, accompanied by pronounced red fluorescence. To determine the freshness of seafood without compromising the food or necessitating complex sample pre-treatment procedures, they used a smartphone to capture images of the smart tags affixed to the food sample packaging and then analyzed the RGB values of these images.

The same group employed a molecular engineering strategy to develop a series of phenothiazine-cyanovinyl-based fluorescence probes (**12a**, **12b**, and **12c**) for efficient detection of cadaverine detection (Fig. 13A).[50] The sensing study commenced with the phenothiazine-3-aldehyde moiety; however, the overlap in emission spectra between the sensor and the product formed upon reaction with cadaverine necessitated improving the sensing performance through substituent engineering. The sensor **12a** was first synthesized from phenothiazine-3-aldehyde and 2-pyridin-4-ylacetonitrile. Although **12a** demonstrated good sensing performance, its sensitivity (LoD = 83.6 nM) and reaction time (35 min) were

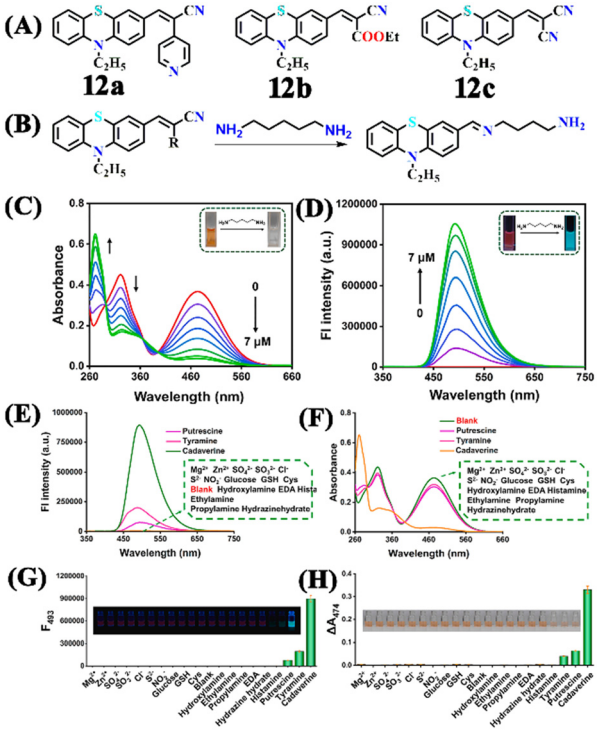

Fig. 13 (A) The structure of sensors **12a–c** and (B) the proposed mechanism of cadaverine sensing. (C) The UV-visible absorption and (D) fluorescence emission spectra of **12c** at different concentrations of cadaverine. The observed (E) electronic absorption and (F) fluorescence emission spectra for **12c** in the presence of cadaverine and various competitive analytes and (G and H) their corresponding histogram demonstrate the high selectivity for **12c** for cadaverine (inset: photographs for visual colour changes imaged in room light and under UV light). Reproduced with permission from ref. 50. Copyright 2023, Elsevier.

suboptimal. Using **12b**, they enhanced the sensitivity (LoD = 62.5 nM) by including a more potent electron-withdrawing group, although there was no enhancement in response time. Ultimately, they developed a superior sensor **12c** by including two potent nitrile groups. **12c** showed ultra-fast (~16 s) reaction and exceptional sensitivity (LoD = 3.9 nM) for cadaverine. These sensors exhibited distinct colour changes from dark red to bright cyan (Fig. 13C and D). They proposed that cadaverine sensing follows a nucleophilic addition/elimination mechanism (Fig. 13B). Additionally, **12c** test strips were developed for the portable and visual detection of cadaverine vapour. The study showed a fluorescence colour change from crimson to cyan (Fig. 13D). **12c** displayed an excellent selectivity for cadaverine in the coexistence of other analytes (Fig. 13E–H). This allows for precise measurement of cadaverine vapour levels through RGB colour mode analysis. An excellent capacity for non-destructive, non-contact, and visual screening of meat freshness on site was established by the **12c** test strips, which were used for determining the freshness of actual beef samples.

Utilizing the same molecular engineering strategy, Wang and colleagues synthesized a series of fluorescent probes (**13a**, **13b**, and **13c**) derived from benzothiazole for the

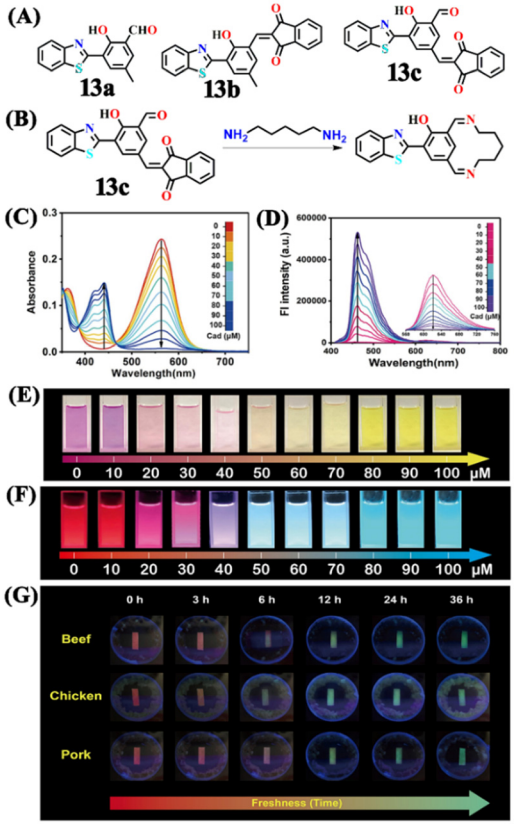

Fig. 14 (A) The structure of sensors **13a–c** and (B) the proposed cadaverine sensing mechanism cyclic Schiff base formation. (C) The UV-visible absorption and (D) fluorescence emission spectra of **13c** at different concentrations of cadaverine and their corresponding visual colour changes were imaged under (E) daylight and (F) UV light. (G) Photographs of **13c** tags used for monitoring the freshness of beef, chicken, and pork stored at 25 °C recorded at different exposure times. Reproduced with permission from ref. 51. Copyright 2024, Elsevier.

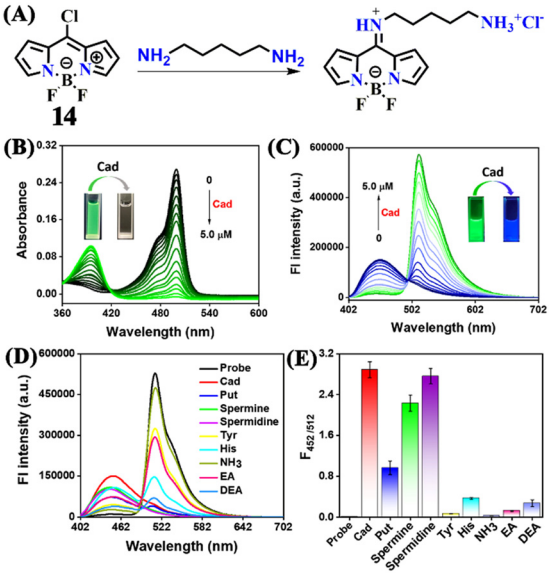

Fig. 15 (A) The structure of sensor **14** and its reaction with cadaverine yield a blue-emitting product. The ratiometric UV-visible absorption (B) and fluorescence emission (C) changes were observed for **14** after the gradual addition of cadaverine (inset: the photographs of colour changes observed). (D) The differential fluorescence sensing properties of **14** for different amine analytes and (E) corresponding histogram. Reproduced with permission from ref. 52. Copyright 2023, Elsevier.

detection of cadaverine and putrescine by nucleophilic condensation to produce Schiff bases (Fig. 14A and B).[51] They began sensitivity studies from **13a** and further sensitivity and response time were enhanced by replacing various recognition groups. The extended conjugated sensor **13c** with dual-reaction sites showed a rapid sensing response (~15 minutes), excellent selectivity, and high sensitivity (LoD = 70 nM). The absorption intensity of **13c** at λ = 560 nm progressively decreased on increasing the concentration of cadaverine and a new peak at λ = 441 nm emerged, which resulted in a notable colour shift from purple to pale yellow (Fig. 14C and E). The strong fluorescence emission peak of **13c** at λ = 620 nm attenuated along with a new emission peak at λ = 462 nm was progressively increased; this produced a visual colour change from red to fluorescence green (Fig. 14D and F). It was hypothesized that cadaverine sensing follows an amine-induced reversed Knoevenagel condensation reaction resulting in a cyclic Schiff base formation. Furthermore, cadaverine and putrescine were detected on-site within five minutes using a portable smartphone-based fluorescence device. The **13c**-loaded portable test strips were efficiently used as smartphone-compatible fluorescent labels to detect cadaverine and putrescine in meat samples at various temperatures (Fig. 14G). This enabled consumers and other participants in the food supply chain to quickly and visually assess the freshness of genuine beef, chicken, and pork items.

Last year, Min *et al.* developed a BODIPY-based sensor **14** for detecting cadaverine and other BAs (Fig. 15).[52] In the presence of cadaverine, **14** underwent a sequential nucleophilic addition–elimination reaction to yield a blue-emitting product and a ratio metric fluorescence response from green to blue (Fig. 15A). The initial absorption spectra of **14** at λ = 499 nm gradually decreased. In comparison, a new absorption peak at λ = 395 nm progressively intensified (Fig. 15B). Similarly, the initial emission band at λ = 452 nm progressively shifted to λ = 452 nm (Fig. 15C). **14** showed exceptional sensing capabilities, characterized by remarkable selectivity (Fig. 15D and E), elevated sensitivity, a low LoD = 5.1 nM, and a rapid reaction time. Moreover, **14** was integrated into a flexible and portable sensing platform to detect BAs vapour, exhibiting a significant fluorescence shift from green to blue. The sensor device can non-destructively check meat freshness in real time and this was readily observable by the naked eye.

Li and the team created an innovative three-in-one sensor **15** used for BAs sensing through olfactory, colorimetric, and fluorescent signals (Fig. 16A).[53] **15** rapidly reacts with BAs *via* nucleophilic substitution, which resulted in high sensitivity for detection with a LoD of 0.03 μM. The reaction of **15** with BAs produces a side product ethanethiol, a compound with

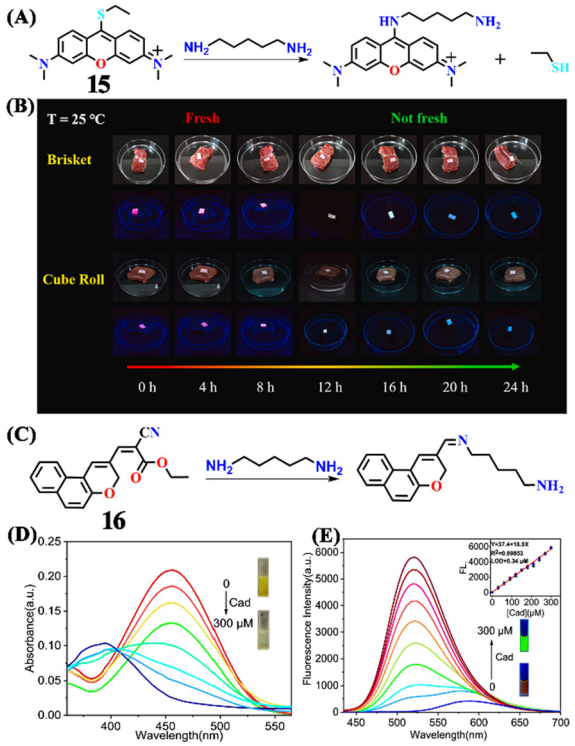

Fig. 16 (A) The proposed mechanism of cadaverine sensing by **15** and (B) **15** loaded fluorescent paper was used to monitor the freshness of beef at 25 °C and at different exposure times. (C) The structure of sensor **16** and its reaction with cadaverine resulted in Schiff base formation. The observed changes in (D) UV-visible absorption and (E) fluorescence emission spectra of **16** upon increased addition of cadaverine (inset: the photographs of colour changes observed before and after the mixing of cadaverine). Reproduced with permission from ref. 53 and 54. Copyright 2024, Elsevier.

distinct odours that serves as an olfactory alert. Cadaverine, spermidine, spermine, and benzylamine exhibited the fastest reactions with **15**. The UV-visible absorption spectrum of **15** showed a peak at λ = 574 nm which disappeared upon the reaction with BAs and a new peak appeared at λ = 426 nm. In the emission spectra, these BAs completely quenched the emission band of sensor **15** at λ = 605 nm, while producing a blue-shifted emission peak at λ = 533 nm. This resulted in a ratiometric fluorescence response, characterized by a distinct fluorescence transition from red to green. The team has also embedded **15** in a low-cost, portable paper format, enabling real-time and easy-to-use monitoring of beef freshness (Fig. 16B).

In a recent study, Li *et al.* reported a benzo[h]chromene derivative-based sensor **16** exhibiting exceptional optical sensitivity towards 12 different BAs.[54] They specifically investigated the sensing propensity of **16** for cadaverine. The interaction between **16** and cadaverine produced a Schiff base derivative (Fig. 16C), altering the molecular charge distribution. This interaction induced pronounced changes in colorimetric and fluorescence properties, facilitating the recognition of cadaverine. Notably, the absorption peak at λ = 454 nm exhibited a redshift, while the fluorescence emission peak at λ = 520 nm showed an upward shift with increasing cadaverine concentration (Fig. 16D and E). The LoD for cadaverine was determined to be 0.34 μM. The probe was immobilized on filter paper to create a sensing label capable of visually indicating fish freshness to enhance practical applicability. By integrating this label with a smartphone-based platform, the researchers developed a rapid and accurate visual detection system for assessing the freshness of salmon.

In addition to the small-molecule fluorescence sensors, several other types of sensors including metal–organic frameworks (MOF),[55] covalent organic frameworks (COFs),[56,57] and fluorescent dyes incorporated hybrid materials,[58] have been developed and successfully employed for the detection of cadaverine. The overall focus of this article is to explicitly highlight reactivity-based small-molecule fluorescence sensors for cadaverine detection and thus, determine the food freshness. To know more about the sensing properties of these sensors, readers can refer to the appropriate references cited herein.

3. Conclusions and outlook

In summary, we have highlighted the recent development of small-molecule-based ratiometric fluorescent sensors used to sense cadaverine, a relevant biogenic amine. Table 1 summarizes the fluorescent sensing properties of various small-molecule sensors explained in this article. Ultra-trace sensing and *in situ* monitoring of cadaverine concentrations is a vital method to know food freshness and spoilage. In recent years, several fluorescent sensors have been developed to sense cadaverine, including organic and inorganic polymers, hybrid materials, luminescent quantum dots, and nanomaterials.[55–58] However, small-molecule-based ratiometric fluorescent sensors gained substantial research attention owing to their great advantages such as facile synthesis, structural diversity, functional tunability, and good sensing performance. Recently a wide variety of small-molecule-based ratiometric fluorescence sensors have been designed based on different types of fluorophores including rhodamine, fluorescein, coumarin, BODIPY, and naphthalimides.

Most of these sensors exhibit selective sensing performances for closely related BAs, while a few are highly selective towards cadaverine. The high selectivity of sensors for cadaverine has been achieved by functionalizing the core-fluorescent unit with reactive functional groups such as aldehyde, anhydride, ester, dicyanovinyl, and so on. These functional fluorophores quickly react with the primary amine group of cadaverine, which results in a product different from the initial sensors. Consequently, notable changes in the absorption and fluorescence emission spectra of sensors. Various reaction mechanisms such as anhydride–amine reaction, deprotonation reaction, ring-opening reaction, Schiff base reaction, aza-Michael addition, chromophore reaction, aminolysis reaction, and Meisenheimer complex

Table 1 The sensing properties of small-molecule-based fluorescence sensors **1–16** are discussed in this article

Sensors structure	Emission maxima λ_{em} (nm)	Sensing medium	Binding interactions	Limit of detection (LoD)	Ref.
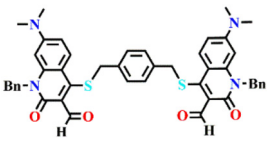 **1a**	537	MeOH-buffered water (50 mM HEPES, 240 mM NaCl, pH = 7.4 before dilution in MeOH)	Through the formation of a bis-iminium ion	μM	33
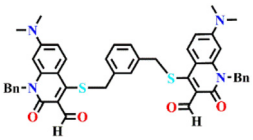 **1b**	537	MeOH-buffered water (50 mM HEPES, 240 mM NaCl, pH = 7.4 before dilution in MeOH)	Through the formation of a bis-iminium ion	μM	33
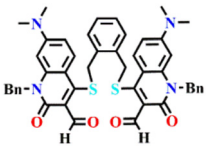 **1c**	537	MeOH-buffered water (50 mM HEPES, 240 mM NaCl, pH = 7.4 before dilution in MeOH)	Through the formation of a bis-iminium ion	μM	33
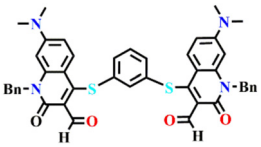 **1d**	537	MeOH-buffered water (50 mM HEPES, 240 mM NaCl, pH = 7.4 before dilution in MeOH)	Through the formation of a bis-iminium ion	μM	33
 **1e**	537	MeOH-buffered water (50 mM HEPES, 240 mM NaCl, pH = 7.4 before dilution in MeOH)	Through the formation of a bis-iminium ion	μM	33
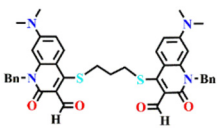 **1f**	537	MeOH-buffered water (50 mM HEPES, 240 mM NaCl, pH = 7.4 before dilution in MeOH)	Through the formation of a bis-iminium ion	μM	33
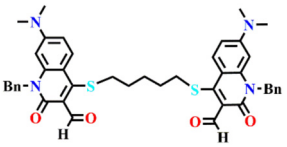 **1g**	537	MeOH-buffered water (50 mM HEPES, 240 mM NaCl, pH = 7.4 before dilution in MeOH)	Through the formation of a bis-iminium ion	μM	33
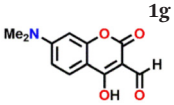 **2**	470	Buffered aqueous solution (50 mM HEPES, pH 7.4)	Formation of imines	μM	39
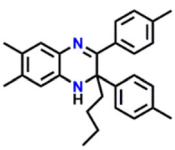 **3**	560	Filter paper strips	Deprotonation by amines	ppb	30
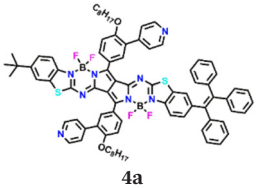 **4a**	700 and 525	Dioxane	B–N bonds and imine sites react with amines	ppb	41

Table 1 *(continued)*

Sensors structure	Emission maxima λ_{em} (nm)	Sensing medium	Binding interactions	Limit of detection (LoD)	Ref.
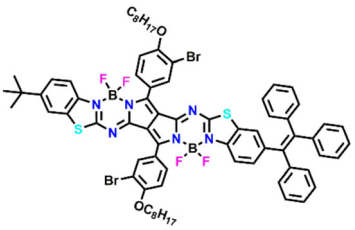 4b	700 and 525	Dioxane	B–N bonds and imine sites react with amines	ppb	41
 4c	700 and 525	Dioxane	B–N bonds and imine sites react with amines	ppb	41
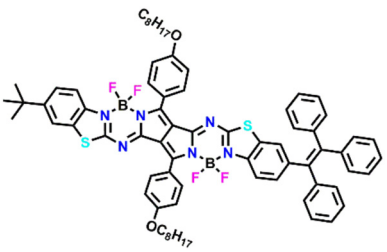 4d	700 and 525	Dioxane	B–N bonds and imine sites react with amines	ppb	41
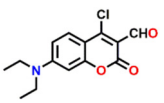 5	475	EtOH/PBS (v/v = 3/7, pH = 8.2)	Nucleophilic substitution and condensation reaction	nM	43
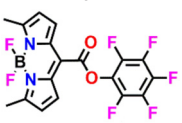 6a	615	CH_3CN	Ester-to-amide conversion	nM	44
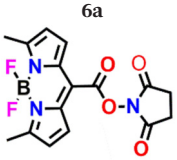 6b	648	Aqueous buffered solutions (10 mM PBS, pH 7.4, 1% CH_3CN)	Ester-to-amide conversion	—	44
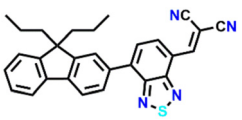 7a	600	DCM	Aza-Michael addition	ppb	45
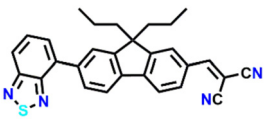 7b	500	DCM	Aza-Michael addition	ppb	45

Table 1 *(continued)*

Sensors structure	Emission maxima λ_{em} (nm)	Sensing medium	Binding interactions	Limit of detection (LoD)	Ref.
 8	573	ACN	Nucleophilic substitution	μM	46
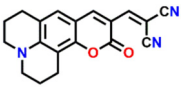 9a	610	DMSO	Aza-Michael addition followed by an elimination reaction	μM	47
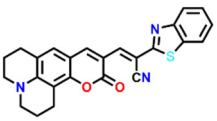 9b	650	DMSO	Aza-Michael addition followed by an elimination reaction	nM	47
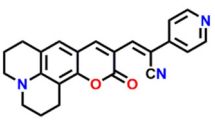 9c	604	DMSO	Aza-Michael addition followed by an elimination reaction	nM	47
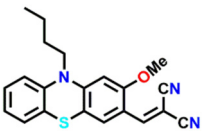 10	Weak band at 704	DMSO	Reversed Knoevenagel condensation reaction	nM	48
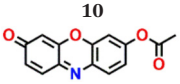 11	592	DMSO/PBS (v/v = 3/7, pH 7.4)	Aminolysis	nM	49
 12a	493	DMSO	Nucleophilic addition/elimination reaction	nM	50
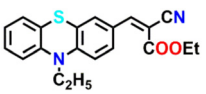 12b	493	DMSO	Nucleophilic addition/elimination reaction	nM	50
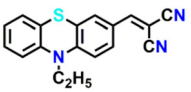 12c	493	DMSO	Nucleophilic addition/elimination reaction	nM	50
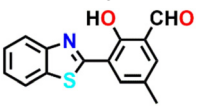 13a	483	—	Nucleophilic condensation generates Schiff bases	nM	51
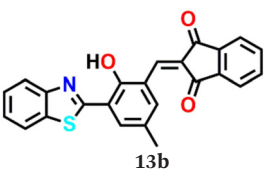 13b	700	—	Nucleophilic condensation generates Schiff bases	nM	51
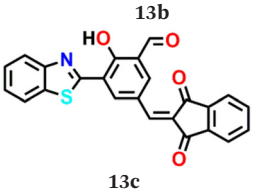 13c	620	—	The reversed-Knoevenagel reaction followed by the formation of a cyclic Schiff base	nM	51

Table 1 *(continued)*

Sensors structure	Emission maxima λ_{em} (nm)	Sensing medium	Binding interactions	Limit of detection (LoD)	Ref.
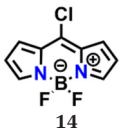 14	512	CH_3CN	Nucleophilic addition followed by a distinctive elimination reaction	nM	52
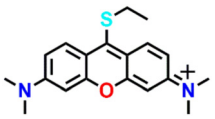 15	605	Aqueous solution with 1% CH_3CN (v/v)	Nucleophilic substitution reaction of amines	μM	53
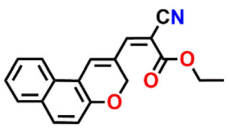 16	520	EtOH/H_2O (4/6, v/v) solution	Schiff base product	μM	54

formation have been hypothetically proposed for cadaverine sensing.

The use of small-molecule-based fluorescence chemosensors for sensing biogenic amines, particularly cadaverine, is immense. However, various issues limit the sensors described herein, and these issues must be adequately addressed to develop practically useful small-molecule fluorescent sensors for cadaverine sensing. Many of the sensors presented here lack high selectivity for cadaverine. They often sense multiple biogenic amines along with cadaverine. For instance, the sensor that detects cadaverine also interacts strongly with putrescine and other primary amines. This can result in false positive sensing responses. As said above, small-molecule-based sensors provide opportunities to tune the structure and functionality to improve the sensing properties. Therefore, the selectivity for cadaverine sensing can be improved to a greater extent by carefully introducing the right reactive functional groups and placing these functional groups at a similar distance to the length of cadaverine analytes; thereby, high selectivity for cadaverine can be achieved. Another issue is the reaction time to produce noticeable spectral changes for analyte detection. Most sensors react with the target analyte for a few seconds to minutes. The reaction time of the sensor can be enhanced by designing the fluorophores with complementary reactive functional groups.

The ratiometric sensing responses are also an issue with discrete small-molecule fluorescence sensors. One equivalent of the sensor is needed to sense one equivalent of the analyte (stoichiometric binding) and thus, poor sensitivity for detection. However, this issue has recently been addressed by using supramolecular polymer sensors.[59,60] This provides an extended polymeric network-like structure in which the fluorescent moieties are connected through multiple non-covalent interactions. So, one equivalent of analyte can completely quench the fluorescence emission of the supramolecular polymer through long-range electronic communications. Consequently, the sensitivity of sensors can be enhanced to multi-fold. Reversible sensing is another requirement to meet the practical use of any sensors. However, the ratiometric sensors fail to show reversible sensing due to their chemical conversion upon binding with the target analytes. The reversibility of the sensor could be achievable if the bonding between the sensor and analyte is kinetically labile. The initial structure of sensors can be regenerated if the appropriate external stimulus is used to break the bonding between the sensor and analyte.

In a nutshell, we have exemplified various small-molecule fluorescent and colorimetric sensors, their photophysical properties, cadaverine sensing mechanism, and their applications in determining food freshness are described in great detail. We believe that the examples presented in this article will provide new directions for designing fluorescent chemosensors for selectively sensing cadaverine over other biogenic amines and device fabrication for practical feasibility in the future.

Data availability

No new data were generated or analysed as part of this review.

Conflicts of interest

There are no conflicts to declare.

Acknowledgements

We are grateful to the Indian Institute of Technology Palakkad (ERG research grant 2023-168-CHY-SHS-ERG-SP to SS), and Science and Engineering Research Board (EMEQ research grant EEQ/2023/000386 to SS), India, for financial support.

Notes and references

1 M. R. Grossman, *Eur. Food Feed Law Rev.*, 2016, **11**, 63–66.
2 V. Varlet and X. Fernandez, *Food Sci. Technol. Int.*, 2010, **16**, 463–503.
3 M. P. Doyle and M. C. Erickson, *Poult. Sci.*, 2006, **85**, 960–973.
4 M. A. Hussain, *Foods*, 2016, **5**, 21; I. A. Rather, W. Y. Koh, W. K. Paek and J. Lim, *Front. Pharmacol.*, 2017, **8**, 830.
5 B. Liang and D. Scammon, *Int. J. Nonprofit Volunt. Sect. Mark.*, 2006, **21**, 227–241.
6 A. Naila, S. Flint, G. Fletcher, P. Bremer and G. Meerdink, *J. Food Sci.*, 2010, **75**, R139–R150.
7 A. Pacquit, J. Frisby, D. Diamond, K. T. Lau, A. Farrell, B. Quilty and D. Diamond, *Food Chem.*, 2007, **102**, 466–470.
8 C. Shang, G. Wang, M. He, X. Chang, J. Fan, K. Liu, H. Peng and Y. Fang, *Sens. Actuators, B*, 2017, **241**, 1316–1323.
9 B. Del Rio, B. Redruello, D. M. Linares, V. Ladero, P. Ruas-Madiedo, M. Fernandez, M. C. Martin and M. A. Alvarez, *Sci. Rep.*, 2019, **9**, 120.
10 G. Jairath, P. K. Singh, R. S. Dabur, M. Rani and M. Chaudhari, *J. Food Sci. Technol.*, 2015, **52**, 6835–6846.
11 M. A. Alvarez and M. V. Moreno-Arribas, *Trends Food Sci. Technol.*, 2014, **39**, 146–155.
12 H. A. Kim, H. S. Lee, T. H. Shin, J. Y. Jung, W. Y. Baek, H. J. Park, G. Lee, M. J. Paik and C. H. Suh, *Lupus*, 2018, **27**, 930–938.
13 M. Ikeda, T. Yoshii, T. Matsui, T. Tanida, H. Komatsu and I. Hamachi, *J. Am. Chem. Soc.*, 2011, **133**, 1670–1673.
14 M.-Z. Dai, Y.-L. Lin, H.-C. Lin, H.-W. Zan, K.-T. Chang, H.-F. Meng, J.-W. Liao, M.-J. Tsai and H. Cheng, *Anal. Chem.*, 2013, **85**, 3110–3117.
15 K. V. Kumudavally, A. Shobha, T. S. Vasundhara and K. Radhakrishna, *Meat Sci.*, 2001, **59**, 411–415.
16 H. S. Marks and C. R. Anderson, *J. Chromatogr. A*, 2005, **1094**, 60–69.
17 M. Awan, *Open Chem.*, 2008, **6**, 229–236.
18 S. Leonardo and M. Campàs, *Microchim. Acta*, 2016, **183**, 1881–1890.
19 T. Soga, Y. Jimbo, K. Suzuki and D. Citterio, *Anal. Chem.*, 2013, **85**, 8973–8978.
20 N. A. Rakow, A. Sen, M. C. Janzen, J. B. Ponder and K. S. Suslick, *Angew. Chem., Int. Ed.*, 2005, **44**, 4528–4532.
21 X. Mei and C. Wolf, *J. Am. Chem. Soc.*, 2006, **128**, 13326–13327.
22 C. Zhang and K. S. Suslick, *J. Am. Chem. Soc.*, 2005, **127**, 11548–11549.
23 X. Wu, L. Zeng, B.-Q. Chen, M. Zhang, J. Rodrigues, R. Sheng and G.-M. Bao, *J. Mater. Chem. B*, 2019, **7**, 5775–5781.
24 L. Zeng, H. Zeng, L. Jiang, S. Wang, J.-T. Hou and J. Yoon, *Anal. Chem.*, 2019, **91**, 12070–12076.
25 X. Hu, H. Zeng, T. Chen, H.-Q. Yuan, L. Zeng and G.-M. Bao, *Sens. Actuators, B*, 2020, **319**, 128282.
26 C. Duan, M. Won, P. Verwilst, J. Xu, H. S. Kim, L. Zeng and J. S. Kim, *Anal. Chem.*, 2019, **91**, 4172–4178.
27 L. Jiang, T. Chen, E. Song, Y. Fan, D. Min, L. Zeng and G.-M. Bao, *Chem. Eng. J.*, 2022, **427**, 131563.
28 J. Chung, K. M. K. Swamy and J. A. Kim, *Bull. Korean Chem. Soc.*, 2021, **42**, 107–110.
29 D. G. Müller, E. Q. Oreste, M. G. Heinemann, D. Dias and F. Kessler, *Eur. Polym. J.*, 2022, **175**, 111221.
30 L. Wang, X. Ran, H. Tang and D. Cao, *Dyes Pigm.*, 2021, **194**, 109634.
31 A. Gupta, *ChemistrySelect*, 2019, **4**, 12848–12860.
32 R. Tejpal, M. Kumar and V. Bhalla, *Sens. Actuators, B*, 2018, **258**, 841–849.
33 K. Secor, J. Plante, C. Avetta and T. Glass, *J. Mater. Chem.*, 2005, **15**, 4073–4077.
34 S. Mallick, F. Chandra and A. L. Koner, *Analyst*, 2016, **141**, 827–831.
35 R. Roy, N. R. Sajeev, V. Sharma and A. L. Koner, *ACS Appl. Mater. Interfaces*, 2019, **11**, 47207–47217.
36 R. Jia, W. Tian, H. Bai, J. Zhang, S. Wang and J. Zhang, *Nat. Commun.*, 2019, **10**, 795.
37 S. Jeon, T.-I. Kim, H. Jin, U. Lee, J. Bae, J. Bouffard and Y. Kim, *J. Am. Chem. Soc.*, 2020, **142**, 9231–9239.
38 E. K. Feuster and T. E. Glass, *J. Am. Chem. Soc.*, 2003, **125**, 16174–16175.
39 B. Lee, R. Scopelliti and K. Severin, *Chem. Commun.*, 2011, **47**, 9639–9641.
40 P. Alam, N. L. C. Leung, H. Su, Z. Qiu, R. T. K. Kwok, J. W. Y. Lam and B. Z. Tang, *Chem. - Eur. J.*, 2017, **23**, 14911–14917.
41 L. Li, W. Li, L. Wang, H. Tang, D. Cao and X. Ran, *Sens. Actuators, B*, 2020, **312**, 127953.
42 L. Wang, H. Ding, H. Tang, D. Cao and X. Ran, *Anal. Chim. Acta*, 2020, **1135**, 38–46.
43 B. Zhu, L. Jiang, T. Chen, G. M. Bao, L. Zeng, X. Hu and H. Q. Yuan, *Dyes Pigm.*, 2021, **186**, 108963.
44 S. Jeon, T. Il Kim, H. Jin, U. Lee, J. Bae, J. Bouffard and Y. Kim, *J. Am. Chem. Soc.*, 2020, **142**, 9231–9239.
45 G. Zhang, A. S. Loch, J. C. M. Kistemaker, P. L. Burn and P. E. Shaw, *J. Mater. Chem. C*, 2020, **8**, 13723–13732.
46 F. Monteiro-Silva, C. Queir, A. Leite, T. Rodr, J. Rojo, R. C. Martins, A. M. G. Silva and M. Rangel, *Molecules*, 2021, **26**, 1–15.
47 H. Ye, S. Koo, B. Zhu, Y. Ke, R. Sheng, T. Duan, L. Zeng and J. S. Kim, *Anal. Chem.*, 2022, **94**, 15423–15432.
48 L. Jiang, H. Ye, D. Ma, J. Rodrigues, R. Sheng and D. Min, *Analyst*, 2022, **147**, 923–931.
49 J. Zhang, J. Zhou, T. Zhang, Y. Tang and L. Zeng, *Spectrochim. Acta, Part A*, 2023, **296**, 122647.
50 H. Ye, Y. Ke, W. Li, B. Zhu, L. Jiang, X. Hu and L. Zeng, *Anal. Chim. Acta*, 2023, **1254**, 341125.
51 J. Zhang, Y. Yang, L. Zeng and J. Wang, *Food Chem.*, 2024, **436**, 137769.
52 L. Jiang, B. Zhu, Y. Shao, H. Ye, X. Hu and D. Min, *Dyes Pigm.*, 2023, **220**, 111771.
53 D. Wang, X. Ding, J. Xie, J. Wang, G. Li and X. Zhou, *Anal. Chim. Acta*, 2024, **1285**, 342025.

54 Y. Li, X. Jiang, Y. Li, X. Yan, L. Tang, X. Sun, K. Zhong, X. Li and J. Li, *Food Chem.*, 2024, **458**, 140239.
55 T. Leelasree and H. Aggarwal, *J. Mater. Chem. C*, 2022, **10**, 2121–2127.
56 G. Das, B. Garai, T. Prakasam, F. Benyettou, S. Varghese, S. K. Sharma, F. Gándara, R. Pasricha, M. Baias, R. Jagannathan, N. Saleh, M. Elhabiri, M. A. Olson and A. Trabolsi, *Nat. Commun.*, 2022, **13**, 1–12.
57 J.-Y. Yue, Z.-X. Pan, L.-P. Song, W.-J. Yu, H. Zheng, J.-C. Wang, P. Yang and B. Tang, *Anal. Chem.*, 2023, **95**, 17400–17406.
58 M. Ikeda, T. Yoshii, T. Matsui, T. Tanida, H. Komatsu and I. Hamachi, *J. Am. Chem. Soc.*, 2011, **133**, 1670–1673.
59 B. Gole, S. Shanmugaraju, A. K. Bar and P. S. Mukherjee, *Chem. Commun.*, 2011, **47**, 10046–10048.
60 S. Shanmugaraju, H. Jadhav, R. Karthik and P. S. Mukherjee, *RSC Adv.*, 2013, **3**, 4940–4950.